Korean J. Chem. Eng., 38(6), 1231-1239 (2021)
DOI: 10.1007/s11814-021-0806-4

pISSN: 0256-1115
eISSN: 1975-7220

Contributions of post-synthesized mesopore structures of ferrierite zeolite for gas-phase dimethyl ether carbonylation activity

Thi Xuan Nguyen‡, Ji Won Moon‡, Hyun Seung Jung‡, Gui Young Han†, and Jong Wook Bae†

School of Chemical Engineering, Sungkyunkwan University (SKKU), 2066 Seobu-ro, Suwon, Gyeonggi-do 16419, Korea
(*Received 4 February 2021 • Revised 8 April 2021 • Accepted 11 April 2021*)

Abstract−Mesoporous ferrierite zeolite (FER) synthesized by a post-desilication method was applied for a gas-phase dimethyl ether (DME) carbonylation to confirm the contributions of the newly formed mesoporous structures above 10 nm in size. The distribution of surface acidic sites and extent of coke deposition was significantly altered, resulting in showing different catalytic activity and stability, which were mainly caused by the post-synthesized larger mesopores on the FER. The newly formed mesoporous structures in the range of 5-40 nm on the pristine seed-derived FER (SFER) with a Si/Al molar ratio of 10.4 were largely changed by a desilication/recrystallization duration, and the mesopores significantly increased the surface acidic sites with similar extent of crystallinity even with a lower Si/Al ratio of 6.7-8.6. The increased strong acidic sites corresponding to Brønsted acid sites after an optimal desilication duration for ~3 h on the mesoporous SFER (m-SFER(3)) were mainly responsible for an increased DME carbonylation activity with smaller formation of coke precursors due to facile mass transport phenomena through its lager mesopores.

Keywords: Gas-phase Carbonylation, Dimethyl Ether (DME), Mesoporous Ferrierite (m-FER), Post-desilication, Methyl Acetate (MA)

INTRODUCTION

Solid acidic zeolites having uniform microporous structures have been known to be active for various heterogeneous catalytic reactions, for example, petroleum refining processes and petrochemical syntheses [1,2], which are further applied to synthesize value-added chemicals like methanol, dimethyl ether (DME) and acetates [1-5] from various renewable feedstock. Among various zeolites, ferrierite (FER) possesses typical 8-membered ring (8-MR) channel structures cross-linked with 10-membered ring (10-MR) channels [6] with their respective micropore sizes of 4.2×5.4 and 3.5×4.8 Å. The FER has been reported to have superior activity for gas-phase carbonylation of DME [7-10] or selective skeletal isomerization of *n*-pentene and *n*-butene on the more active 8-MR channels [11]. Furthermore, to overcome mass transfer limitation in the zeolite micropores, the application of mesoporous zeolites has been largely proposed by using simple desilication methods with alkaline solution under specific conditions [12-14], which cause a significant leaching of framework Si atoms [15-19] by forming heterogeneous mesoporous structures in the ZSM-5 (MFI) [17-20], mordenite (MOR) [21], faujasite (FAU) [22], and FER [23]. For example, the optimal Si/Al molar ratio was reported in the range of 25-50 to form desilicated mesoporous ZSM-5 structures [16,17,20,24]. The Al atoms play an important role as a mesopore-generating species during dissolution step because Al atoms with negatively charged AlO_4^- natures in each zeolite framework can prevent the extraction of neighboring Si atoms. Therefore, the usage of a concentrated NaOH solution (~1.0 mol/L) is essential to effectively form the mesopore structure on the zeolites having Si/Al molar ratio smaller than 25 [25]. The FER having a lower Si/Al ratio below 10 [26] with relatively larger 10-MR channels can help the diffusion of molecules [23,26]; however, the appearance of 6-MR channels (along with [101] direction) with its micropore size of 0.25 nm seems to be small to diffuse out larger organic molecules. Therefore, the newly created mesopores on the FER are apt to shorten the diffusion path length by overcoming the diffusion limitations [23]. However, over-leaching treatments with NaOH solution can cause significant disintegration of zeolite structures. Some recent reports to synthesize hierarchically structured micro-mesoporous H-form FER (Si/Al molar ratio of 27) generally follow two successive post-treatment steps, such as partial dissolution step to form its nanocrystals in NaOH solution and hydrothermal recrystallization step with cetyltrimethyl ammonium bromide (CTAB) as a cationic surfactant to minimize in-situ structural disintegration of FER frameworks such as irregular and excessive structure collapses as the well-reported previous researches [12,27-29]. However, the above stepwise procedures seem to be difficult to form uniform mesoporous structures due to irregular formations of various mesoporous structures and sizes preferentially. Therefore, one-step simple procedure by desilication with NaOH solution and simultaneous recrystallization with CTAB was recently reported for the selective synthesis of mesoporous zeolites [12,30-35].

In the present study, the one-step recrystallization method of commercial FER (Vision Chem.) and home-made seed-derived H-form FER [3-5] having a Si/Al ratio of ~10 were separately used to prepare mesoporous FER through one-step desilication method in

†To whom correspondence should be addressed.
E-mail: gyhan@skku.edu, finejw@skku.edu
‡The authors of N. T. Xuan, J. W. Moon and H. S. Jung equally contributed.

an alkaline medium [12]. The effects of the desilication duration and mesopore structures according to the types of FERs were verified for catalytic performance and structural stability in terms of surface acidity as well as coke deposition during a gas-phase DME carbonylation reaction to methyl acetate (MA), which has not been well investigated till now as far as we know.

EXPERIMENTAL SECTION

1. Synthesis of Mesoporous FERs Using Commercial and Seed-derived FER

For the preparation of mesoporous FERs by a desilication and simultaneous recrystallization method, a commercial NH_4^+-form FER supplied by Vision Chem. having a Si/Al molar ratio of ~10 was used after thermal treatment at 550°C for 3 h under air environment to generate H^+-form FER (denoted as CFER), and home-made seed-derived FER (denoted as SFER) was previously synthesized at a fixed Si/Al ratio of 10.4 with 24 wt% CFER seed at a constant molar ratio of $SiO_2/NaAlO_2/NaOH/water=1.0:0.096:0.15:36$ by the well-known hydrothermal synthesis method as reported in our previous work [3-5]. The detailed synthesis method of the seed-derived FER was as follows: sodium hydroxide (NaOH) with 0.80 g and fumed silica (SiO_2) of 0.80 g were added to 86.4 g deionized water (DIW) and the above mixed solution was stirred at room temperature for 1 h at 500 rpm. After additional vigorous stirring for 1 h, 2.13 g commercial FER seed material (H-form) was added to above mixture, which was further stirred for 11 h. Successively, sodium aluminate ($NaAlO_2$, 1.05 g) was added into the above solution and stirred for 12 h additionally. Finally, the suspension was treated at hydrothermal synthesis temperature of 160 °C in a Teflon tube-lined stainless autoclave for 96 h under a stirring condition. After cooling the synthesis reactor to room temperature, the obtained white gel was filtered at vacuum condition and further washed with 4 L of DIW. Finally, the product was dried overnight at 80 °C followed by thermal treatment at 550 °C for 6 h under an air environment. The SFER was further treated with an ammonium nitrate solution (1.0 mol/L) to prepare NH_4-form FER at 80 °C for 3 h. After several repetitions of the ion-exchange step to form H-form FER, the obtained white powder was thermally treated under air environment at 550 °C for 3 h. For a successive desilication and recrystallization of the FERs, the separate commercial and home-made FERs, cethyltrimethyl ammonium bromide (CTAB, Alfa Aesar) and deionized water were used to synthesize desilicated mesoporous FERs. For more details, 6 g of the parent FER with 3 g of CTAB was mixed with 200 mL of 0.25 mol/L NaOH solution and the mixture was thoroughly stirred for 3 h at room temperature, which was hydrothermally treated at 160 °C for 96 h. The obtained white gel was washed with deionized water until pH of 7 and dried overnight followed by calcination under an air environment at 550 °C for 6 h. The as-prepared desilicated FERs were prepared by a successive ion-exchange treatment for six times with 1.0 mol/L NH_4NO_3 solution. Finally, the NH_4-form FERs were calcined again under air flow at 550 °C for 8 h to form mesoporous H-form FERs, where the desilicated mesoporous FERs were denoted as m-CFER(x) and m-SFER(x) with x digit for a different desilication time (h), separately.

2. Measurements of carbonylation activity and characterization procedures

Catalytic performance and its stability for a selective gas-phase carbonylation of DME to MA was obtained by using a fixed-bed tubular reactor having an inner diameter of 9 mm on the fresh desilicated m-FERs. Prior to catalytic performance measurement, the catalyst with 0.4 g was pretreated under N_2 flow at 500 °C for 1 h to get rid of any contaminant and water adsorbed. The reaction condition was fixed to T=220 °C, P=1.0 MPa and higher space velocity (SV) of 6,000 h^{-1} with a feed gas composition of DME/CO/N_2=5/45/50 for the reaction duration of 50 h on stream to verify the effects of mesoporosity of the FERs. The methanol, DME, MA and hydrocarbons formed were analyzed by on-line gas chromatography (GC, Younglin YL6100) equipped with a flame ionization detector (FID) with a DBWAX capillary column. DME conversion and product distribution were measured by using total carbon-balance by assuming with insignificant coke depositions on the m-FERs. Deactivation rate for ~50 h (R_D, %/h) was also measured by using the values of DME conversion at maximum and steady-state as follows.

Deactivation rate (R_D, %/h)=(maximum DME conversion (%) − DME conversion at a steady-state (%))/ (its duration (h) between the maximum and steady-state value)

The patterns of wide-angle X-ray diffraction (XRD) on the fresh m-FERs were measured by a Bruker X-ray diffractometer (D8 Advance) equipped with Cu Kα radiation (0.15406 nm) operated at 40 kV and 100 mA at a fixed scanning rate of 4°/min in the range 2θ=5-60° to measure the characteristic XRD patterns of the desilicated m-FERs. With the help of X-ray fluorescence (XRF) analysis by using a Bruker S4 instrument operating at 60 kV and 150 mA, the bulk Si/Al molar ratio on the fresh m-FERs was also measured. To measure the specific surface area and average pore diameter, N_2 adsorption-desorption isotherm on the fresh m-FERs was characterized by using an ASAP2020 instrument at a liquid N_2 temperature of −196 °C with the help of Brunauer-Emmett-Teller (BET) method and Barrett-Joyner-Halenda (BJH) method from the desorption branch of N_2-sorption isotherm, respectively.

To verify surface acidic properties such as the numbers and types, the adsorption properties with a probe molecule of pyridine and NH_3 on the fresh m-FERs were separately measured after pretreating the sample at 500 °C for 1 h under vacuum condition to remove water and contaminants adsorbed. The adsorbed pyridine molecules on a shelf-supported thin pellet were measured by Fourier transform infrared spectroscopy (FT-IR) analysis (Py-IR) by using a Frontier MIR/FIR spectrometer (PerkinElmer) installed with an MCT detector. The temperature-programmed desorption of ammonia (NH_3-TPD) was analyzed with 50 mg of the fresh m-FER sample in the range of 50-700 °C under He flow by a thermal conductivity detector (TCD) installed in a BELCAT-M instrument. To verify the amount of coke precursors formed on the used m-FERs with its types, temperature-programmed surface reaction analysis with hydrogen (H_2-TPSR) was further investigated in the temperature range of 200-1,000 °C after the sample pretreatment at 300 °C for 1 h under He flow, where the effluent gases were monitored with a Quadropole mass spectrometer (QMS, QMA200) by on-

line measuring the fragments of CH_4 with a mass number (m/z) of 15. The outermost surface morphology of the fresh m-FERs was further characterized by field emission scanning electron microscopy (FESEM) with a JSM-7000F instrument operated at 30 kV. The local surface morphology and mesopores distribution on the fresh m-FERs were also verified by transmission electron microscopy (TEM) with a JEM-2100F instrument operated at 200 kV. The amounts of deposited coke precursors on the used FERs were quantified by measuring TGA weight loss (%) above 400 °C (ramping rate of 10 °C/min under air environment by a TGA 55 model (TA instrument) and by comparing its derivative thermogravimetry (DTG) patterns.

RESULTS AND DISCUSSION

1. Characteristics of m-FERs Prepared by desilication and recrystallization method

Bulk XRD patterns of the fresh m-FERs before and after desilication are displayed in Fig. 1. After the deciliation of the pristine FERs, the crystallinity of the m-FERs was significantly decreased with an increase of desilication duration due to the leaching of the FER's frameworks by a direct attack of OH^- formed from basic NaOH solution [12]. However, the characteristic FER structures were clearly preserved even after the desilication of the m-FERs. Interestingly, the relatively larger characteristic peak intensity on the m-SFER compared to the m-CFER suggests the preservation of higher crystallinity of the seed-derived FER even after desilication

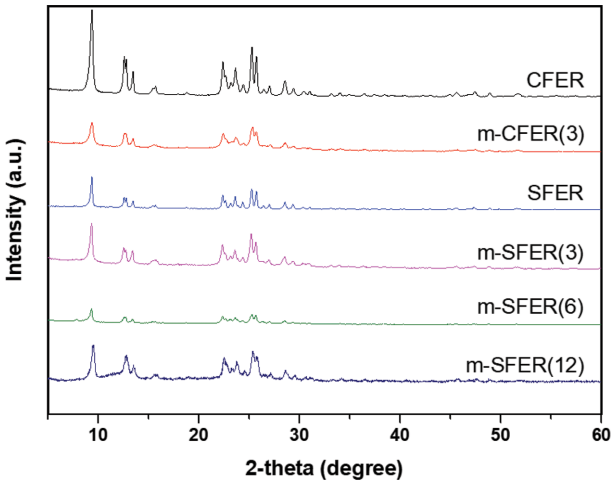

Fig. 1. Wide-angle XRD patterns of the pristine and modified mesoporous FERs.

Table 1. Catalytic performance on the modified mesoporous FERs with their bulk and surface properties

Catalyst[a] (desilication duration, h)	XRF	XRD[b]	N_2 sorption[c]	NH_3-TPD[d]	Py-IR[e]	Active site[f]	Catalytic activity[g]	TPSR (g, $\times 10^8$)[h]	TGA[i]
	Si/Al ratio	$D_{crystal}$ (%)	S_g (meso)/ Pv/Dp	W/M/S (total) (mmol/g)	B/L ratio	B sites (8 MR) (mmol/g)	$X_{DME}/S_{MA}/R_D$	$\alpha/\beta/\gamma$ phase (total)	Coke (mg_{coke}/g)
CFER	10.3	100	283(38)/0.24/3.4	0.94/0.35/0.56 (1.85)	16.5	0.53	12.1/95.6/0.07	0.05/0.05/0.23 (0.33)	54.8
m-CFER(3)	7.3	35	316(157)/0.37/4.7	0.57/0.48/0.57 (1.63)	6.2	0.54	13.0/90.5/0.31	1.72/0.39/1.06 (3.17)	124.3
SFER	10.4	25	308(35)/0.20/2.7	0.64/0.55/0.35 (1.54)	26.7	0.19	4.2/95.3/0.12	0.04/0.03/0.01 (0.08)	56.9
m-SFER(3)	6.7	45	325(159)/0.44/5.4	0.83/0.22/0.62 (1.68)	7.0	0.59	16.5/95.0/0.06	0.73/0.34/0.74 (1.81)	63.7
m-SFER(6)	7.3	15	304(139)/0.50/6.6	0.59/0.47/0.44 (1.50)	5.0	0.34	6.3/60.2/0.05	0.62/1.03/0.89 (2.54)	75.6
m-SFER(12)	8.6	42	315(107)/0.41/5.1	0.72/0.29/0.29 (1.30)	1.4	0.26	4.7/57.9/0.05	0.82/0.37/0.54 (1.73)	54.8

[a]Ferrierte (FER) zeolites are denoted as the CFER and SFER for the commercial and seed-derived FER, respectively. After desilication for x hours, the mesoporous FER zeolites are, respectively, denoted as m-CFER(x) and m-SFER(x) as well.

[b]Relative degree of crystallinity (denoted as $D_{crystal}$) of the mesoporous FERs was denoted by calculating the integrated peak area of the most intense peak assigned to $2\theta=9.3^o$ (largest peak) based on the 100% crystallinity of the reference CFER.

[c]S_g, P_v, and D_P denotes specific surface area (m^2/g) with that of mesopore (meso), pore volume (cm^3/g), and average pore diameter (nm), respectively.

[d]Weak (W), medium (M) and strong (S) acid sites on the fresh FERs measured by NH_3-TPD analysis were assigned to the peak at ~200, ~350 and 350-600 °C, respectively.

[e]Relative ratio of Brønsted(B) to Lewis(L) acid sites was measured by Py-IR analysis, which were assigned to the absorption peak appeared at 1,542 cm^{-1} for B sites and peak at 1,454 cm^{-1} for L sites, respectively.

[f]The number of Brønsted (B) acid sites in the 8 membered-ring (8-MR) channels was quantified by the equation of [(strong acid sites (S) from NH_3-TPD) – (B sites from Py-IR)] with the assumption of B sites in the 10-MR channels only measured by Py-IR analysis.

[g]Catalytic performances such as DME conversion (X_{DME}, mol%) and MA selectivity (S_{MA}, mol%) are presented with the average values for the reaction duration of 10 h after 40 h on stream at a steady-state, and the deactivation rate (R_D, %/h) was calculated by using the difference between maximum and stead-state conversion divided by its total duration.

[h]Types of the deposited cokes and their relative amounts on the used FERs measured by TPSR experiments were defined as α, β and γ-phase coke precursors appeared at the respective hydrogenation temperatures of ~450, ~550, and ~900 °C, which can be separately assigned to surface carbidic carbon species, amorphous carbons, and heavy cyclic polyaromatic hydrocarbons.

[i]Amounts of coke precursor depositions on the mesoporous FERs after DME carbonylation (mg_{coke}/g_{cat}) were quantified by TGA profiles by calculating the weight loss in the range of 400-1,000 °C (assigned to various surface coke precursors).

by recrystallization of the FER's defect sites [3-5]. The crystallinity of the post-synthesized mesoporous m-FERs with two different CFER and SFER significantly altered the type and number of acidic sites, morphology and Si/Al ratio, which possibly resulted in changing a gas-phase DME carbonylation activity and stability [7]. As summarized in Table 1, the Si/Al molar ratio on the desilicated m-FERs was largely decreased in the range of 6.7-8.6 from 10.3-10.6 on the parent FERs. The significantly decreased Si/Al ratio on the m-FERs after desilication altered their physicochemical properties, resulting in increasing defect sites such as the stronger Brønsted acid sites [7]. However, the optimal m-SFER(3) treated by desilication for 3 h having the smallest Si/Al ratio of 6.7 showed a relatively higher crystallinity as well as well-developed mesopore structure. Based on the XRD peak intensity and relative crystallinity as shown in Fig. 1 and Table 1, the longer desilication duration more than 3 h was responsible for the decreased crystallinity by suppressing the active Brønsted acid sites in the mesoporous m-SFER as confirmed by the lower relative crystallinity of 15-45% with the maximum value of 45% on the m-SFER(3). On the m-SFER(6), the characteristic peaks of FER were significantly decreased due to a lower crystallinity ($D_{crystal}$=15%) with structural collapses of the FER frameworks under the basic OH^- environment. However, the disintegrated FER structures seem to be recrystallized again with the help of CTAB on the m-SFER(12) as confirmed by a higher crystallinity ($D_{crystal}$=42%), where the CTAB seems to play an important role as a structure directing agent [3-5] at a longer desilication duration for 12 h by increasing the crystallinity as supported by an observed intense peak intensity as well. The specific surface areas on the m-FER were observed in the range of 304-325 m^2/g with a relatively larger surface area on the mesoporous m-SFER compared to the pristine CFER (283 m^2/g) due to the preferential formation of mesoporous structures on the m-SFER (Table 1). The mesoporous surface area on the m-SFER was increased after the desilication and recrystallization, for example, from 35 m^2/g on the SFER to 159 m^2/g on the m-SFER(3), and the surface area was obviously decreased with an increase of desilication duration to 107 m^2/g on the m-SFER(12). Similar trends of pore volume and average pore diameter were also observed on the m-SFER, for example, the separate values of 0.44 cm^3/g and 5.4 nm on the m-SFER(3) compared to those of 0.20 cm^3/g and 2.7 nm on the pristine SFER. The preferential formation of mesoporous structures on the m-SFER compared to the m-CFER was generally responsible for the larger surface area, pore volume (0.37 cm^3/g on the m-CFER and 0.41-0.50 cm^3/g on the m-SFER) and average pore diameter (4.7 nm on the m-CFER and 5.1-6.6 nm on the m-SFER), which was attributed to the facile desilication and recrystallization of the home-made SFER. As shown in Fig. 2, typical mesoporous structures with type IV (Fig. 2(a)) and microporous structures of the FER zeolite were clearly observed on the m-SFER with their pore size distributions in the range of 5-40 nm, which was found to be much larger on the m-SFER(3) as shown in Fig. 2(b).

The crystallinity and defect sites of the m-FERs largely changed surface acidity and strength by altering the amount of weak, medium and strong acid sites assigned to different desorption temperatures of the adsorbed NH_3 molecules in the range of 100-600 °C [7] and the results are displayed in Fig. 3. As summarized in Table

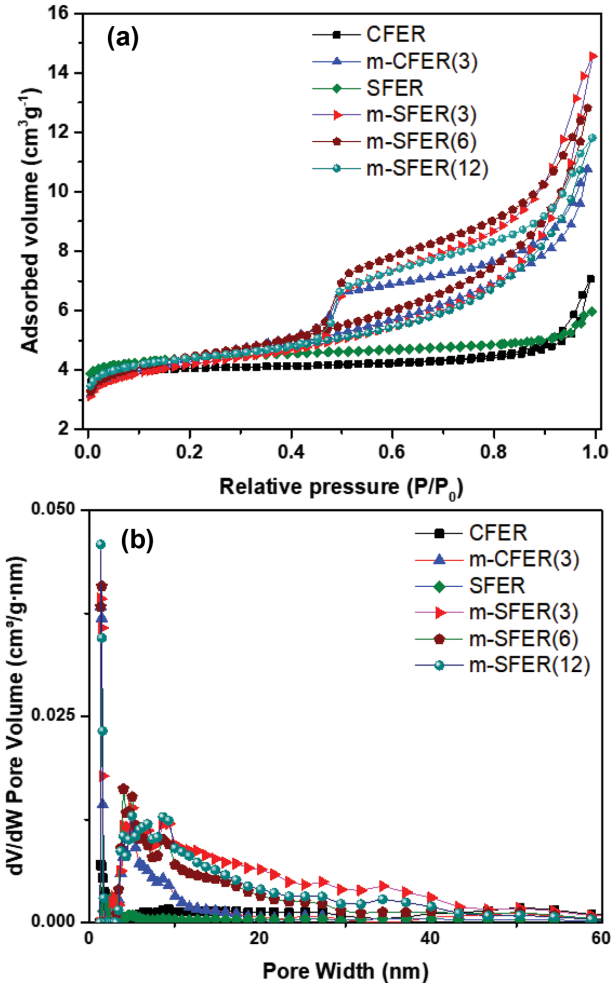

Fig. 2. (a) N_2 adsorption-desorption isotherms and (b) pore size distribution of the fresh mesoporous FER zeolites.

1, the number of weak and medium acidic sites on the FERs was found to be in the range of 0.57-0.94 and 0.22-0.55 mmol/g with a maximum desorption peak temperature at ~211 °C on the m-SFER(3) after the desilication treatment, which can be assigned to the molecular adsorption of NH_3 on the acidic surfaces mainly. However, the strong acidic sites assigned to the peaks at 350-600 °C with its maximum desorption temperatures of 376-429 °C, which are corresponding to the active Brønsted acid sites [3-5], were significantly increased on the optimized m-SFER(3) with the value of 0.62 mmol/g. After desilication for the mesopore generations, the desorption temperatures on the strong acid sites were decreased on both CFER and SFERs by simultaneously increasing those strong acidic sites. Those desorption temperatures on both CFER and SFER were found to be 429 °C, which were decreased to 376 °C on the m-CFER(3) and 410 °C on the m-SFER(3). The desorption temperature was further decreased to ~395 °C on the m-SFER(6) and m-SFER(12). Interestingly, the amounts of the strong acidic sites were increased up to 0.62 on the m-SFER(3) from 0.35 mmol/g on the SFER, while an excessive desilication revealed a significant decrease of the strong acidic sites in the range of 0.27-0.44 mmol/g due to severe structural collapses of the SFER as confirmed by TEM

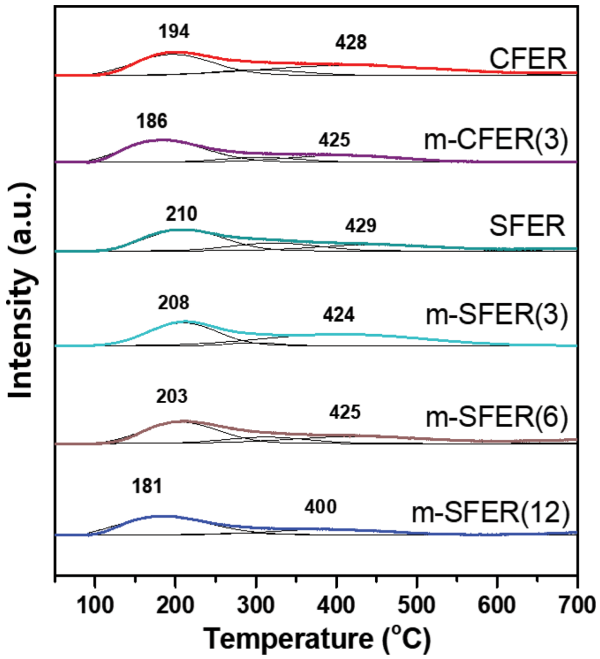

Fig. 3. NH_3-TPD profiles with different characteristic acidic sites on the fresh mesoporous FERs.

and XRD analysis. It suggests that the desilication and recrystallization method for preparing the mesoporous SFERs are effective to enhance the numbers of the active strong acidic sites as well as to decrease less active medium acidic sites on the m-SFER(3) with that value of 0.22 mmol/g. The weak and medium acidic sites on the m-FERs seem to have smaller activity for a gas-phase carbonylation of DME, where those acidic sites can be affected by the FER's crystalline morphology. The pristine plate-like FER structures [12] were obviously observed on the CFER and m-SFER(3) as measured by SEM analysis (Fig. 4). The characteristic FER structures were significantly disintegrated on the m-SFER(12) due to the significant structural collapse, which caused its lower crystallinity as shown in Fig. 4(D). The newly formed mesoporous structures on the desilicated m-FERs were clearly observed by TEM analysis as shown in Fig. 5. The m-SFER(3) as displayed in Fig. 5(D) revealed the selective formations of more homogeneously-distributed mesopores with its sizes of ~50 nm compared to the m-CFER(3) having less homogeneous mesopore structures with its sizes of ~20 nm (Fig. 5(B)) formed from the pristine CFER (Fig. 5(A)), where those mesoporous structures seem to be grown on the [100] direction of FER crystallite [12,23,26]. Compared with the pristine SFER (Fig. 5(C)), more uniformly distributed mesopores were observed on the m-SFER(3) after an adequate desilication duration. How-

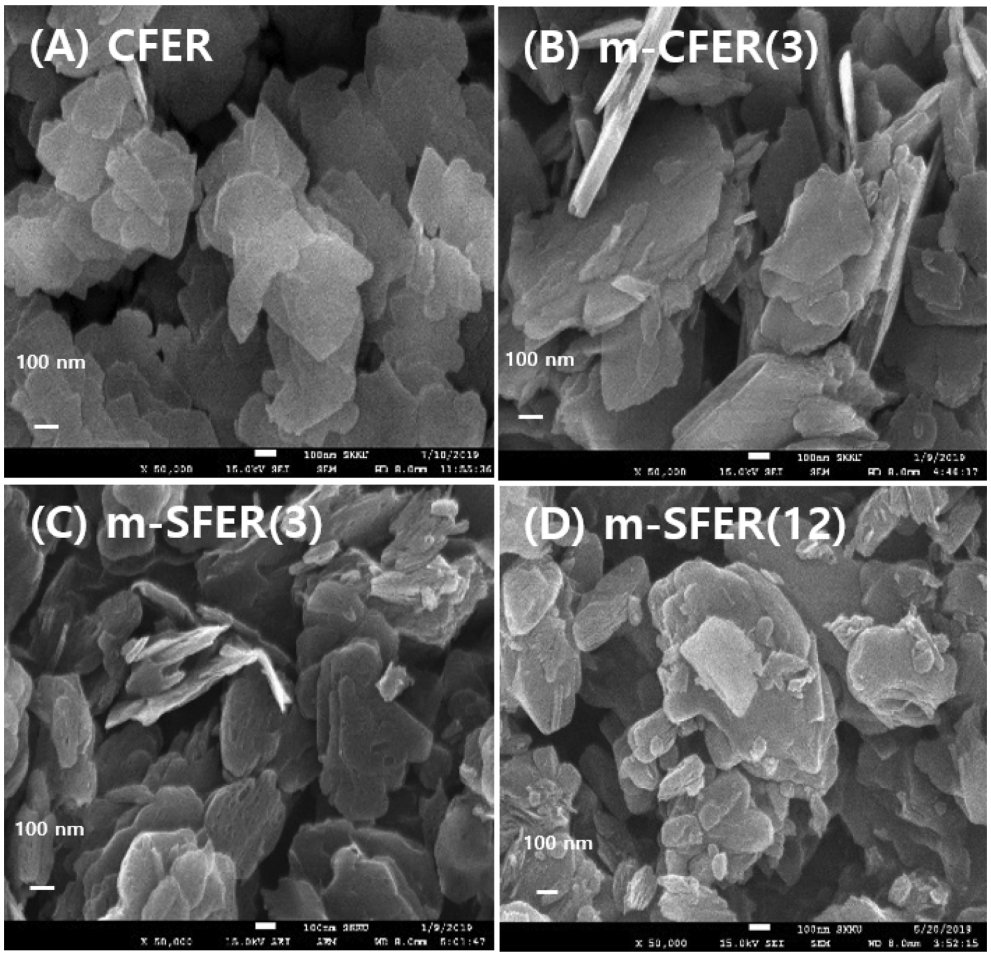

Fig. 4. FESEM images of the fresh (A) CFER, (B) m-CFER(3), (C) m-SFER(3) and (D) m-SFER(12).

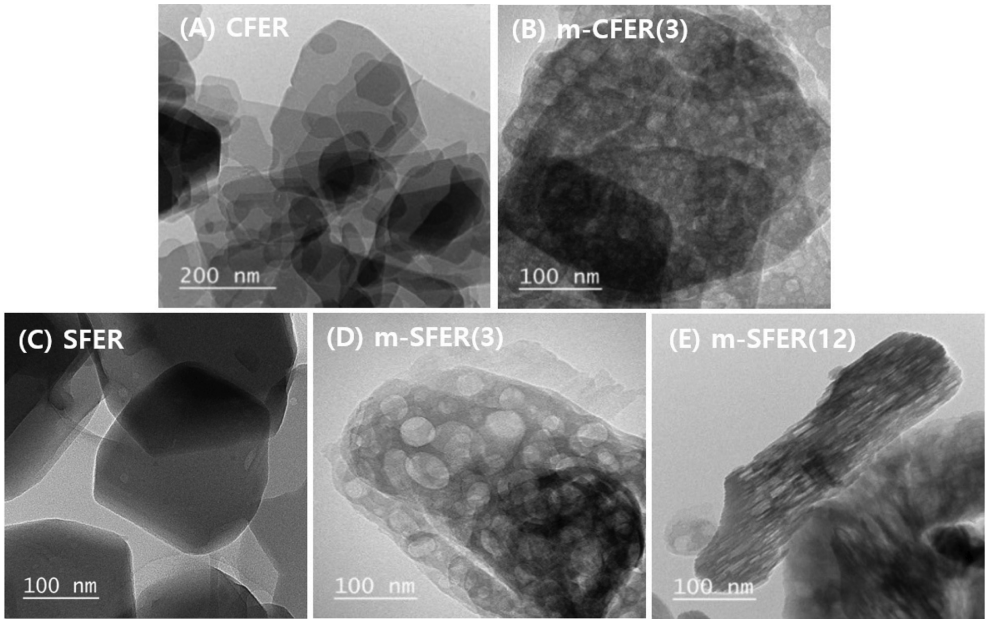

Fig. 5. TEM images of the fresh (A) CFER, (B) m-CFER(3), (C) SFER, (D) m-SFER(3) and (E) m-SFER(12).

ever, those newly formed mesoporous structures on the m-SFER(12) again disintegrated by forming the irregular mesopore sizes as shown in Fig. 5(E), which are in line with the XRD results caused by a significant leaching of FER frameworks under a longer desilication time.

The kinds of acidic sites on the m-FERs were further confirmed by Py-IR analysis and the results are summarized in Table 1. As displayed in Fig. 6, the absorption peaks of Py-IR can be generally assigned to Brønsted (B) acid sites at 1,542 cm^{-1}, Lewis (L) acid sites at 1,454 cm^{-1}, and combined acidic sites (B+L) at 1,480 cm^{-1} [7,36]. The ratios of Brønsted to Lewis acid sites (B/L) were largely altered after desilication on the fresh mesoporous SFER, and less active acidic sites on the mesoporous FERs were generally increased with an increase of desilication duration from CFER and SFER

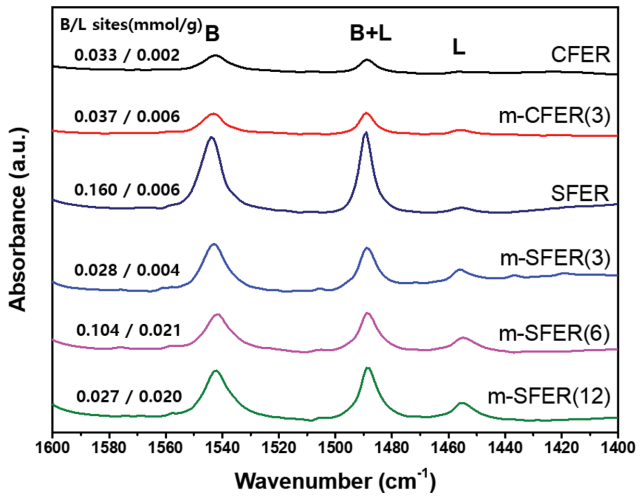

Fig. 6. Py-IR spectra on the fresh FERs carried out at the desorption temperature of 150 °C.

with B/L ratios of 16.5-26.7 to 1.4-7.0 on the mesoporous FERs. Those significantly decreased B/L ratios after desilication on the m-SFER were mainly caused by the generation of defected surface sites as well as incomplete mesopore formation due to the selective adsorption of larger pyridine molecules on the outer surface larger pores. The pyridine probe molecules are difficult to be adsorbed in the smaller micropores of zeolites. Therefore, the quantification derived from Py-IR to measure the amounts of Brønsted (B) acid sites in larger micropores such as 10 or 12 membered-ring (10-MR or 12-MR) channels and external surface acidic sites of zeolites [3-5] as well as NH_3-TPD to measure all acidic sites located in zeolite frameworks was applied to finally quantify Brønsted acid sites in the 8-MR channels of the mesoporous FER. In general, the acidic sites in the 8-MR channels of zeolites are known to be responsible for a higher DME conversion and MA selectivity due to an easy formation of acetyl intermediate (CH_3CO-) on [3-5,7-10,37,38].

The number of Brønsted acid sites measured by Py-IR was generally much smaller than that of NH_3-TPD (strong acidic sites with 0.62 mmol/g), which can be attributed to different affinity of protons, basicity and size differences of ammonia as well as pyridine molecules [39-42]. As summarized in Table 1, the number of the active Brønsted acid sites in the 8-MR channels increased after a proper desilication on the m-SFER(3) with the maximum value of 0.59 mmol/g from 0.19 mmol/g on the pristine SFER, and its small variations between the pristine CFER and m-CFER(3) due to fewer structural disintegrations. Even though the B/L ratios were larger on the pristine FERs (16.5 and 26.7 on the respective CFER and SFER), the mesoporous m-SFER(3) was properly modified to have larger numbers of Brønsted acid sites in the largely-exposed 8-MR channels due to the homogeneously-distributed mesopore formations in the main FER frameworks even with a lower B/L ratio of 7.0. However, the Brønsted acid sites in the 8-MR channels were decreased to 0.26-0.34 mmol/g with an increase of desilication dura-

tion on the m-SFER(6) and m-SFER(12), which was attributed to their severe structural collapse during desilication treatment. Those phenomena were also supported by a higher B/L ratio of 7.0 on the m-SFER(3) compared to m-SFER(6) and m-SFER(12) with the B/L ratio of 1.4-5.0 and m-CFER(3) with that of 6.2 (Table 1), which were smaller than the pristine SFER and CFER with the B/L ratios of 16.5-26.7 due to the formation of less-ordered mesoporous structures causing lower crystallinity as well. In addition, the defect sites on the external surfaces as well as larger sites in the 10-MR channels of the FERs were well related with catalytic deactivation during DME carbonylation [43,44]. Therefore, the larger number of active Brønsted acid sites originating from a higher crystallinity and relatively ordered mesoporous structures on the m-SFER(3) can be responsible for its higher catalytic stability with small amount of coke depositions. As summarized in Table 1 and Fig. 7, total amounts of coke precursors formed on the FER surfaces were found to be relatively lower on the m-SFER(3) with 0.0181 mg/g than that of the m-CFER and m-SFER(6) with 0.0254-0.0317 mg/g, which was mainly attributed to different amounts of the Brønsted acid sites and defect sites measured by various NH_3-TPD, Py-IR, TGA and TPSR analysis in the following section.

2. Effects of Newly Formed Mesopores on m-SFERs to Catalytic Performance

The larger quantity of Brønsted acid sites in the 8-MR channels corresponding to the most active sites for a gas-phase DME carbonylation with its higher crystallinity and well-distributed larger mesopore structures on the m-SFER(3) was responsible for the highest conversion of 16.5% and MA selectivity of 95.0% with much smaller deactivation rate of 0.06%/h even at a higher space velocity. It was mainly attributed to the smaller defect sites by showing a higher B/L ratio of 7.0 with the relatively ordered mesoporous structures for enhancing mass transfer rate [13,14] as well. Interestingly, the much lower DME conversions with 4.7-6.3% and MA selectivity of 57.9-60.2% on the m-SFER(6) and m-FER(12) were attributed to severe structural collapses of the active 8-MR channels of SFERs by an excess exposure under a basic desilication condition with an abundant formation of methanol byproduct from the beginning of reaction. The relatively lower DME conversions of 12.1-13.0% on the CFER and m-CFER(3) can be attributed to the restricted mass transfer rate on the plate-like FER surfaces with their irregular mesopore structures compared to the mesoporous m-SFER(3) as summarized in Table 1 and displayed in Fig. 8. On the desilicated commercial m-CFER(3), a faster decrease of DME conversion from the maximum value of 30.0 to 13.0% (deactivation rate of 0.31%/h) with a stable MA selectivity with 90.5% with time on stream (h) can possibly have originated from its unstable mesopore structures on the m-CFER(3), which resulted in easier coke deposition natures. Based on the catalytic activity and stability on the CFERs and SFERs, the positive effects of ordered mesoporous structures were clearly observed on the m-SFER(3) possessing a larger number of active Brønsted acid sites with insignificant deactivation rate even though it showed a smaller B/L ratio compared to the pristine SFER.

To further verify the roles of post-synthesized mesoporous structures on the m-SFER(3), the analysis of TEM, H_2-TPSR and TGA was carried out and the results are displayed in Fig. 5 and Fig. 7 as well as summarized in Table 1. The characteristic plate-like FER crystallites with size of ~0.5 μm have been known to be effectively desilicated to form mesoporous structures [3-5,12], and the ordered regular pore sizes of ~50 nm on the m-SFER(3) and irregular pore sizes of ~20 nm on the m-CFER(3) were clearly observed. The

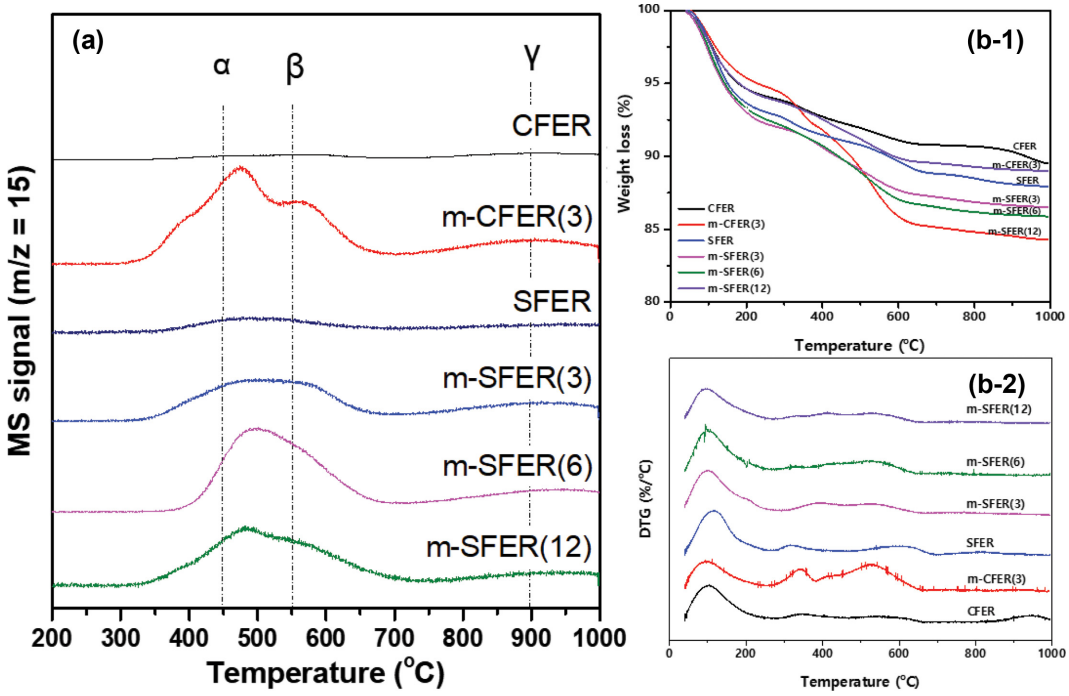

Fig. 7. (a) TPSR patterns monitored by methane fragment (m/z = 15) with mass spectrometer, and (b-1) TGA patterns on the used FERs with (b-2) DTG patterns measured in the temperature range of 50-1,000 °C.

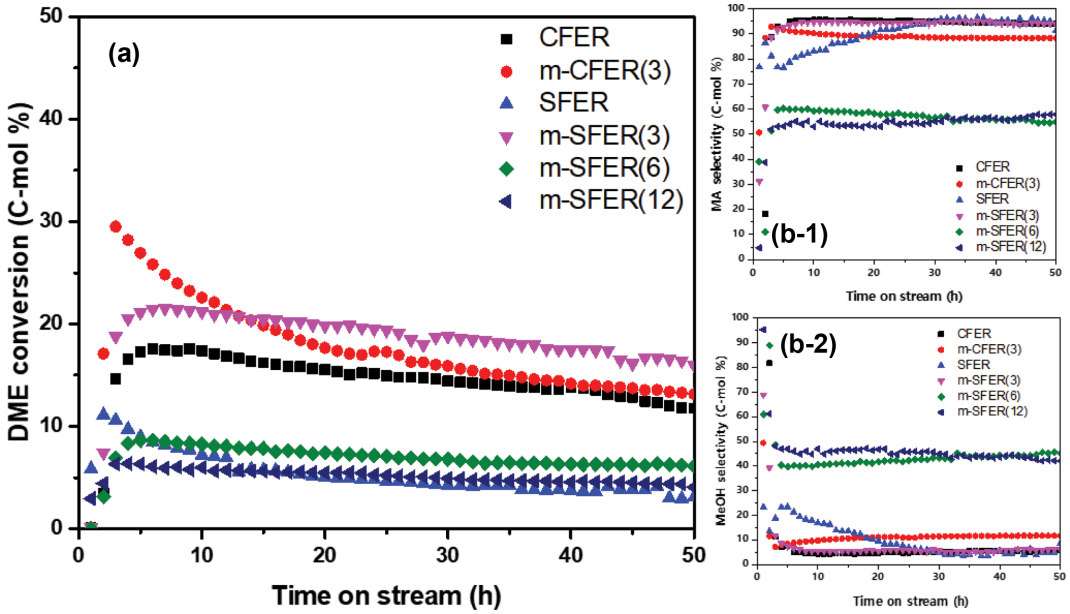

Fig. 8. (a) DME conversion with time on steam on the mesoporous FERs, and (b-1) methyl acetate (MA) selectivity with (b-2) methanol (MeOH) selectivity.

mesoporous structures formed by desilication and recrystallization were more clearly observed on the m-SFER than m-CFER, which seems to be attributed to the easier insertion of CTAB into the SFER having a larger surface area of 308 m^2/g compared to the CFER with that of 283 m^2/g by enhancing the extent of recrystallization as well as by causing less formation of Lewis acid sites (generally assigned to the extra framework aluminum (EFAL) sites), where EFAL sites seem to play an important role as defect sites for coke deposition [12]. The deposited coke precursors formed on the FERs measured by TPSR analysis (Fig. 7(a)) can be categorized with the α, β, and γ-phase cokes according to the hydrogenation temperature. The H_2-TPSR peak at ~450 °C was assigned to surface carbidic carbons as α-form cokes, the peak at ~550 °C was for β-form cokes as surface amorphous hydrocarbons, and the peak at ~900 °C was for γ-form cokes for inactive surface carbons originating from heavy cyclic polyaromatic hydrocarbons possibly [45]. On the desilicated mesoporous m-SFERs, the total deposited cokes were found to be larger in the range of 0.0181-0.0254 mg/g than that of the pristine SFER with 0.0008 μg/g, which was analyzed by H_2-TPSR analysis and the results are summarized in Table 1. Interestingly, the α-form surface cokes were found to be similar on all the desilicated m-SFERs irrespective of their desilication time in the range of 0.0073-0.0082 μg/g compared to that of the mesoporous m-CFER(3) with 0.0172 μg/g, where the trends of β-form and γ-form cokes formed on the m-SFERs were found to be similar. Although the relatively larger amounts of coke precursors were deposited on the mesoporous m-SFER(3) compared to the pristine SFER (0.0008 μg/g), the observed much higher DME conversion of 16.5% and robust catalytic stability with a lower deactivation rate of 0.06%/h were attributed to well-developed regular mesoporous structures with relatively homogeneous size distributions and larger mesoporous cavity (larger mesopore surface area of 159 m^2/g on the m-SFER(3) than that of 35 m^2/g on the SFER) by enhancing the mass transfer rate. The similar phenomena were also observed from TGA and DTG results as summarized in Table 1 and displayed in Fig. 7(b). Absolute weight losses above 400 °C assigned to the removal of coke precursors [5,46,47] were slightly larger on the most active m-SFER(3) with 63.7 mg_{coke}/g due to the selective coke depositions on the outer surface acidic sites [3-7], which were found to be much larger than the amounts of coke precursors measured by TPSR due to its selective and partial hydrogenation. The increased weight losses on the mesoporous FERs (124.3 mg_{coke}/g on the m-CFER(3) and 75.6 mg_{coke}/g on the m-SFER(6)) compared to the pristine FERs (54.8 mg_{coke}/g on the CFER and 56.9 mg_{coke}/g on the SFER) can be possibly attributed to the combined contributions of inevitable coke depositions on the active sites as well as structural collapse of the m-FERs during a gas-phase DME carbonylation reaction.

The superior catalytic activity and stability on the post-synthesized m-SFER(3) compared to the commercial CFER and pristine SFER were attributed to the highly-distributed mesopore structures and smaller number of defect sites assigned to EFAL sites, which originated from the recrystallization with the help of the copresence of CTAB during desilication step. Finally, the relatively higher and stable gas-phase carbonylation activity of DME to MA on the mesoporous m-SFER(3) (Fig. 8) was well correlated with the number of the active Brønsted acid sites with smaller defect sites of the m-SFERs with the help of relatively ordered regular mesoporous structures, which can further effectively suppress the coke deposition resulting in an insignificant catalyst deactivation.

CONCLUSIONS

The number of acidic sites and newly formed mesopore structures on the m-SFER(3) at an optimal desilication duration of 3 h revealed a higher gas-phase carbonylation activity, which further

suppressed the catalyst deactivation rate due to the copresence of post-synthesized regular mesopore structures with smaller EFAL defect sites on the outer surfaces. The newly formed and highly-distributed mesopore structures in the range of 5-40 nm on the seed-derived m-SFERs with the copresence of CTAB largely altered the quantity of Brønsted acid sites as well as their crystallinity. The increased active strong Brønsted acid sites with smaller defect sites on the mesoporous m-SFER(3) were responsible for an increased gas-phase DME carbonylation activity with smaller deposition of surface coke precursors with the help of post-synthesized mesopore structures.

ACKNOWLEDGEMENTS

The authors would like to sincerely acknowledge the financial support from the National Research Foundation of Korea (NRF) grant funded by the Korea government (Project #: NRF- 2018M3 D3A1A01018009 and NRF-2020R1A2C2006052).

REFERENCES

1. H. Zhang, Q. Guo, L. Ren, C. Yang, L. Zhu, A. X. Meng, C. Li and F. Xiao, *J. Mater. Chem.*, **21**, 9494 (2011).
2. S. Kasipandi and J. W. Bae, *Adv. Mater.*, **31**, 1803390 (2019).
3. H. S. Jung, H. Ham and J. W. Bae, *Catal. Today*, **339**, 79 (2020).
4. S. Y. Park, C. H. Shin and J. W. Bae, *Catal. Commun.*, **75**, 28 (2016).
5. H. Ham, H. S. Jung, H. S. Kim, J. Kim, S. J. Cho, W. B. Lee, M. J. Park and J. W. Bae, *ACS Catal.*, **10**(9), 5135 (2020).
6. P. Sarv, B. Wichterlova and J. Cejka, *J. Phys. Chem. B*, **102**, 1372 (1998).
7. J. H. Kim, H. Ham, H. S. Jung, Y. Wang, Y. He, N. Tsubaki, S. J. Cho, G. Y. Han and J. W. Bae, *Catal. Sci. Technol.*, **8**, 3060 (2018).
8. B. Li, J. Xu, B. Han, X. Wang, G. Qi, Z. Zhang, C. Wang and F. Deng, *J. Phys. Chem. C*, **117**, 5840 (2013).
9. A. Bhan, A. D. Allian, G. J. Sunley, D. J. Law and E. Iglesia, *J. Am. Chem. Soc.*, **129**, 4919 (2007).
10. P. Cheung, A. Bhan, G. J. Sunley and E. Iglesia, *Angew. Chem. Int. Ed.*, **45**, 1617 (2006).
11. J. Li, J. Qiu, Y. Sun and Y. Long, *Micropor. Mesopor. Mater.*, **37**, 365 (2000).
12. X. Cheng, T. Cacciaguerra, D. Minoux, J. P. Dath, F. Fajula and C. Gérardin, *Micropor. Mesopor. Mater.*, **260**, 132 (2018).
13. J. C. Groen, S. Brouwer, L. A. A. Peffer and J. Pérez-Ramírez, *Part. Part. Syst. Charact.*, **23**, 101 (2006).
14. X. Li and D. Wu, *Korean J. Chem. Eng.*, **37**, 216 (2020).
15. S. van Donk, A. H. Janssen, J. H. Bitter and K. P. de Jong, *Catal. Rev. Sci. Eng.*, **45**, 297 (2003).
16. D. P. Serrano, J. M. Escola and P. Pizarro, *Chem. Soc. Rev.*, **42**, 4004 (2013).
17. K. Li, J. Valla and J. Garcia-Martinez, *ChemCatChem*, **6**, 46 (2014).
18. M. Ogura, S. Y. Shinomiya, J. Tateno, Y. Nara, E. Kikuchi and M. Matsukata, *Chem. Lett.*, **29**, 882 (2000).
19. M. H. Jeong, K. S. Park, D. M. Shen, J. W. Moon and J. W. Bae, *Korean J. Chem. Eng.*, DOI:10.1007/s11814-020-0709-9.
20. J. C. Groen, J. C. Jansen, J. A. Moulijn and J. Pérez-Ramírez, *J. Phys. Chem. B*, **108**, 13062 (2004).
21. J. C. Groen, T. Sano, J. A. Moulijn and J. Pérez-Ramírez, *J. Catal.*, **251**, 21 (2007).
22. K. P. de Jong, J. Zecevic, H. Friedrich, P. E. de Jong, M. Bulut, S. Van Donk, R. Keumogne, A. Finiels, V. Hulea and F. Fajula, *Angew. Chem. Int. Ed.*, **49**, 10074 (2011).
23. A. Bonilla, D. Baudouin and J. Pérez-Ramírez, *J. Catal.*, **265**, 170 (2009).
24. K. Möller and T. Bein, *Chem. Soc. Rev.*, **42**, 3689 (2013).
25. D. Verboekend, S. Mitchell, M. Milina, J. C. Groen and J. Pérez-Ramírez, *J. Phys. Chem. C*, **115**, 14193 (2011).
26. X. W. Cheng and Y. C. Long, *Adv. Porous Mater.*, **1**, 136 (2013).
27. Yu. P. Khitev, Yu. G. Kolyagin, I. I. Ivanova, O. A. Ponomareva, F. Thibault-Starzyk, J. P. Gilson, C. Fernandez and F. Fajula, *Micropor. Mesopor. Mater.*, **146**, 201 (2011).
28. Yu. P. Khitev, I. I. Ivanova, Yu. G. Kolyagin and O. A. Ponomareva, *Appl. Catal. A: Gen.*, **441-442**, 124 (2012).
29. I. I. Ivanova and E. E. Knyazeva, *Chem. Soc. Rev.*, **42**, 3671 (2013).
30. R. Chal, T. Cacciaguerra, S. van Donk and C. Gerardin, *Chem. Commun.*, **46**, 7840 (2010).
31. R. Chal, C. Gerardin, M. Bulut and S. van Donk, *ChemCatChem*, **3**, 67 (2011).
32. J. Garcia-Martinez, M. Johnson, J. Valla, K. Li and J. Y. Ying, *Catal. Sci. Technol.*, **2**, 987 (2012).
33. M. Manko, R. Chal, P. Trens, D. Minoux, C. Gerardin and W. Makowski, *Micropor. Mesopor. Mater.*, **170**, 243 (2013).
34. C. Bertrand-Drira, X. W. Cheng, T. Cacciaguerra, P. Trens, G. Melinte, O. Ersen, D. Minoux, A. Finiels, F. Fajula and C. Gerardin, *Micropor. Mesopor. Mater.*, **213**, 142 (2015).
35. Y. Han, P. Pitukmanorom, L. Zhao and J. Y. Ying, *Small*, **7**, 326 (2011).
36. T. Gott and S. T. Oyama, *J. Catal.*, **263**, 359 (2009).
37. D. B. Rasmussen, J. M. Christensen, B. Temel, F. Studt, P. G. Moses, J. Rossmeisl, A. Riisager and A. D. Jensen, *Angew. Chem. Int. Ed.*, **54**, 1 (2015).
38. J. A. Z. Pieterse, S. Veefkind-Reyes, K. Seshan, L. Domokos and J. A. Lercher, *J. Catal.*, **187**, 518 (1999).
39. K. Saravanan, K. S. Park, S. Jeon and J. W. Bae, *ACS Omega*, **3**, 808 (2018).
40. K. Saravanan, B. Tyagi, R. S. Shukla and H. C. Bajaj, *Appl. Catal. B: Environ.*, **172-173**, 108 (2015).
41. H. Li, Z. Fang, J. Luo and S. Yang, *Appl. Catal. B: Environ.*, **200**, 182 (2017).
42. A. Auroux, *Top. Catal.*, **19**(3-4), 205 (2002).
43. H. S. Jung, N. T. Xuan and J. W. Bae, *Micropor. Mesopor. Mater.,* **310**, 110669 (2021).
44. A. A. C. Reule and N. Semagina, *ACS Catal.*, **6**, 4972 (2016).
45. J. Xu, W. Zhou, J. Wang, Z. Li and J. Ma, *Chin. J. Catal.*, **30**, 1076 (2009).
46. F. Goodarzia, I. P. Herrerob, G. N. Kalantzopoulosb, S. Svelleb, A. Lazzarinib, P. Beatoc, U. Olsbyeb and S. Kegnæs, *Micropor. Mesopor. Mater.,* **292**, 109730 (2020).
47. M. V. Morales, K. Góra-Marek, H. Musch, A. Pineda, B. Murray, S. Stefanidis, L. Falco, K. Tarach, E. Ponomareva, J. H. Marsman and I. Melián-Cabrera, *Appl. Catal. A: Gen.*, **562**, 215 (2018).